Manganese-Containing Redox Catalysts for Selective Hydrogen Combustion Under a Cyclic Redox Scheme

Ryan B. Dudek, Yunfei Gao, Junshe Zhang, and Fanxing Li
Dept. of Chemical & Biomolecular Engineering, North Carolina State University, Raleigh, NC 27695

DOI 10.1002/aic.16173
Published online April 16, 2018 in Wiley Online Library (wileyonlinelibrary.com)

Selective hydrogen combustion (SHC) in the presence of light hydrocarbons was demonstrated with a series of Mn-containing mixed oxide redox catalysts in the context of a chemical looping-oxidative dehydrogenation scheme. Unpromoted and 20 wt % Na_2WO_4-promoted Mg_6MnO_8, $SrMnO_3$, and $CaMnO_3$ exhibited varying SHC capabilities at temperatures between 550 and 850°C. Reduction temperature of unpromoted redox catalysts increased in the order $Mg_6MnO_8 < SrMnO_3 < CaMnO_3$. Promotion with 20 wt % Na_2WO_4 resulted in more selective redox catalysts capable of high-temperature SHC. XPS analysis revealed a correlation between suppression of near-surface Mn and SHC selectivity. $Na_2WO_4/CaMnO_3$ showed steady SHC performance (89% H_2 conversion, 88% selectivity) at 850°C over 50 redox cycles. In series with a Cr_2O_3/Al_2O_3 ethane dehydrogenation catalyst, $Na_2WO_4/CaMnO_3$ combusted 84% of H_2 produced while limiting CO_x yield below 2%. The redox catalysts reported can be suitable for SHC in a cyclic redox scheme for the production of light olefins from alkanes. © 2018 American Institute of Chemical Engineers *AIChE J*, 64:3141–3150, 2018

Keywords: chemical looping, oxidative dehydrogenation, redox catalyst, selective hydrogen combustion, olefin

Introduction

Cracking and dehydrogenation processes, which convert alkane feedstocks to high-value, unsaturated hydrocarbons, are of significant importance to the chemical industry. These processes are used to produce light olefins such as ethylene and propylene, two essential chemical building blocks with a combined global production of 220 million metric tons in 2012.[1] The production of polyethylene, ethylene oxide, polypropylene, acrylonitrile, and many other critical industrial intermediates relies on these light olefins as feed chemicals.[2,3] At present, ethylene and propylene are primarily produced via these energy-intensive processes, consuming approximately 8% of total primary energy use in the chemicals sector.[1,4] The increased availability of natural gas in recent years has created an economic incentive to convert ethane and propane into the corresponding alkenes.[5,6] As an alternative to the endothermic cracking and dehydrogenation processes, oxidative dehydrogenation (ODH) offers excellent potential to reduce primary energy consumption and pollutant emissions (CO_2 and NO_x) from olefin production.[7]

Oxidative dehydrogenation has been the subject of substantial research since the early 1990s due to its promising characteristics: (i) the ODH reaction is net exothermic and consumes less energy than steam cracking or catalytic dehydrogenation; (ii) the thermodynamic constraints on cracking and dehydrogenation reactions can be mitigated by oxidizing the hydrogen co-product; (iii) the presence of oxygen minimizes coke deposition and subsequent deactivation of the catalyst.[8–11] In the classical ODH literature, the most well-studied catalyst systems for ethane and propane ODH are those containing vanadium oxide and molybdenum oxide.[12–16] Platinum-group metals have also received attention for the ODH of various alkanes.[17,18] Most ODH reactions are operated between 400 and 700°C and use co-fed gaseous oxygen. Although the ODH scheme provides numerous advantages, the safety concerns with oxygen-hydrocarbon mixing and the cost of O_2 via cryogenic air separation limit its commercial attractiveness. Novel ODH approaches that preserve the advantages of conventional ODH while addressing its limitations are therefore highly desirable.

Chemical looping-oxidative dehydrogenation (CL-ODH) is a process scheme for ODH without the need for gaseous O_2.[19–22] The CL-ODH scheme consists of two process steps in a cyclic reduction-oxidation (redox) mode (Figure 1). In the ODH step, the alkane feedstock is converted to alkene and water by lattice oxygen donated from an oxide-based redox catalyst. The subsequent regeneration step involves re-oxidizing the reduced redox catalyst with air to complete the redox cycle. This regeneration step releases heat, which is stored and transferred by the catalyst particles to satisfy the energetic requirements of the ODH step. Although the overall reaction for CL-ODH is identical to that of conventional ODH (Figure 1), the use of the metal oxide redox catalyst facilitates the separation of oxygen from air and provides lattice oxygen to the ODH reaction in a controlled manner. CL-ODH

Additional Supporting Information may be found in the online version of this article.

Correspondence concerning this article should be addressed to F. Li at fli5@ncsu.edu.

Current address of J. Zhang: School of Chemical Engineering and Technology, Xi'an Jiaotong University, Xi'an, Shaanxi 710049, China

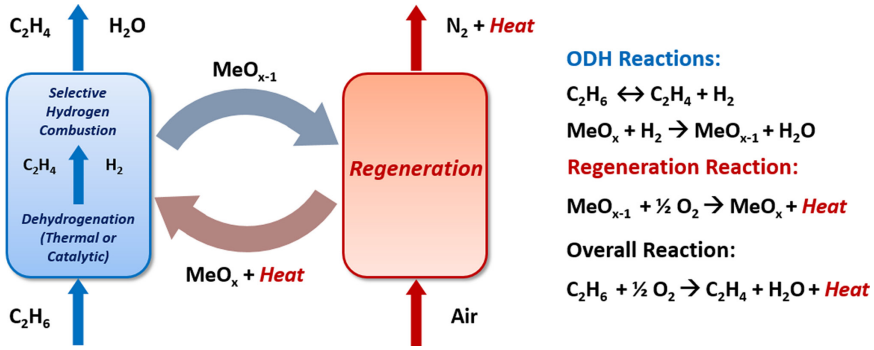

Figure 1. A simplified block flow diagram for the chemical looping-oxidative dehydrogenation scheme.

In this scheme, the ODH (reduction) step at left is comprised of two reactions. The first reaction is dehydrogenation (DH), proceeding either via gas-phase thermal cracking or by heterogeneous catalysis, and the second reaction is selective hydrogen combustion from the products of the dehydrogenation reaction. [Color figure can be viewed at wileyonlinelibrary.com]

eliminates the need for purified O_2 from cryogenic air separation and minimizes explosion hazards from co-feeding oxygen with hydrocarbons. Moreover, the use of lattice oxygen can potentially inhibit non-selective oxidation reactions while reducing energy consumption and CO_2/NO_x emissions.[7] Due to the critical role of the redox catalyst, its performance (i.e., activity, selectivity, oxygen capacity, and durability) is the key to realizing the aforementioned advantages of CL-ODH.[23–25]

As presented in Figure 1, the ODH step of the overall CL-ODH process can be implemented by coupling alkane dehydrogenation with selective hydrogen combustion (SHC). This approach to CL-ODH involves the use of the redox catalyst to selectively combust the hydrogen co-product from alkane dehydrogenation (DH); the DH reaction can occur either catalytically via a co-catalyst or through thermal cracking. The redox catalyst is not intended to interact with the fed alkane and should be relatively inert toward hydrocarbons in general, a difference which distinguishes this method from catalytic ODH.[21,26–29] Combustion of the hydrogen co-product not only provides heat to the endothermic dehydrogenation reaction but also can shift the dehydrogenation equilibrium toward the product side. Early studies of the catalytic DH + SHC approach investigated the use of a Pt-Sn-ZSM-5 dehydrogenation catalyst in the presence of bismuth, indium, and lead oxides or molybdates.[30–33] Rothenberg et al. further explored SHC by cerium oxides in CL-ODH processes, identifying the importance of SHC to achieving improved olefin yields; in the absence of a DH co-catalyst, these studies relied on simulated ethane DH or propane DH effluent streams containing H_2 and olefins.[34–40] However, the attractiveness of these SHC materials is hindered by their high cost (cerium, bismuth, and indium oxides), toxicity (lead, molybdenum, and vanadium oxides), and lack of stability under continuous redox cycles. More recently, Yusuf et al. implemented CL-ODH by coupling thermal cracking of ethane with SHC and reported up to 68% ethylene yield with manganese-containing redox catalysts, which was among the highest yields reported in literature.[22] The use of low-cost and low-toxicity manganese-based redox catalysts is advantageous; however, the reported process relies on high-temperature cracking (800°C and higher) to generate ethylene and hydrogen. High operating temperatures can lead to increased energy consumption and reactor costs as well as challenges in controlling product selectivity due to complex gas-phase reactions. Therefore, extending the SHC properties of manganese-containing materials into the lower-temperature region can potentially provide greater flexibility in CL-ODH process design, especially in combination with the well-established literature on catalytic dehydrogenation.[6]

The current study aims to systematically investigate the SHC properties of three Mn-containing mixed oxides. Mn-containing mixed oxides including perovskite structured $CaMnO_3$ and rock salt structured Mg_6MnO_8 have demonstrated excellent oxygen donation properties for chemical looping.[20,41,42] Our recent work showed that promoting Mg_6MnO_8 with sodium tungstate (Na_2WO_4) results in enhanced selectivity for hydrogen combustion while inhibiting activation of fed ethane or produced ethylene by the metal oxide.[20] Here, we further investigate and extend the effect of Na_2WO_4 promotion for SHC properties to other Mn-containing oxides. Importantly, we determine that SHC properties of Mn-containing oxides can be optimized for specific operating temperature ranges in redox ODH by varying the metal oxide substrate and promoter content. As such, the SHC redox catalysts developed in this study can be suitable for CL-ODH under a variety of operating conditions.

Experimental

Redox catalyst preparation

Six redox catalysts including unpromoted and 20 wt % Na_2WO_4-promoted Mg_6MnO_8, $SrMnO_3$, and $CaMnO_3$ were prepared. Magnesium manganese oxide (Mg_6MnO_8) was synthesized using a wet impregnation method, and 20 wt % Na_2WO_4-promoted Mg_6MnO_8 was further obtained using a second wet impregnation step, both as reported elsewhere.[22] Strontium manganate ($SrMnO_3$) and calcium manganate ($CaMnO_3$) were synthesized via a modified Pechini method.[43] Stoichiometric amounts of $Mn(NO_3)_2{\cdot}4H_2O$ (97.0%, Sigma-Aldrich) and either $Sr(NO_3)_2$ (99.0%, Noah) or $Ca(NO_3)_2{\cdot}4H_2O$ (99.0%, Sigma-Aldrich) were dissolved in deionized water with citric acid (99.5%, Sigma-Aldrich) in a 2.5:1 molar proportion of citric acid to metal ions (Mn^{4+} and either Sr^{2+} or Ca^{2+}). The resulting solution was stirred at 500 rpm and 40°C for 30 min. Next, to aid the formation of a gel, ethylene glycol (99.8%, Sigma-Aldrich) was added to the mixture in a 1.5:1 molar proportion of ethylene glycol to citric acid. The solution was heated to 80°C and stirred at 500 rpm until gel formation, then transferred to an oven and dried overnight at 120°C. Calcination was subsequently conducted in two

steps. First, the gel was heated in the muffle furnace to 450°C at 5°C/min and held for 3 h to burn off nitrates, leaving a uniform metal oxide powder precursor. Second, the powder was calcined in a tube furnace (GSL-15 0X, MTI Corporation) under continuous air flow at 1000°C for 12 h (3°C/min ramping rate). The high temperature led to the formation of perovskite oxide phase $SrMnO_3$ and $CaMnO_3$. To synthesize promoted $SrMnO_3$ or $CaMnO_3$, sodium tungstate (Na_2WO_4) was added to the as-obtained perovskite oxide substrates in the amount of 20 wt % via wet impregnation as described in the previous paragraph, followed by drying overnight at 80°C. Finally, both $Na_2WO_4/SrMnO_3$ and $Na_2WO_4/CaMnO_3$ were calcined at 900°C. All redox catalysts were ground and sieved into the 250–425 μm range for reaction testing. Powders finer than 250 μm were used for characterization techniques.

Redox catalyst characterization

Crystal phases of as-prepared redox catalysts were confirmed via powder X-ray diffraction (XRD) using a Rigaku SmartLab X-ray diffractometer (monochromatic Cu Kα radiation with $\lambda = 0.1542$, operated at 40 kV and 44 mA). XRD patterns were generated over a scanning range of $2\theta = 10°$–$80°$ with 0.05° step size, holding at each step for 3 s. Phases were matched to reference patterns from the International Center for Diffraction Data (ICDD) database in the HighScore Plus software package. Specific surface areas of redox catalysts were obtained via BET analysis of N_2 physisorption isotherms on a Micromeritics ASAP 2020 instrument at 77 K. All samples were degassed at 200°C under vacuum prior to adsorption measurements.

Near-surface compositional information was obtained using X-ray photoelectron spectroscopy (XPS). For each as-prepared redox catalyst, XPS narrow scans were taken for all metal cations present (Mg 2s, Sr 3d, Ca 2p, Mn 2p, Na 1s, W 4f), along with C 1s and O 1s. Scans were also taken for cycled $CaMnO_3$ and $Na_2WO_4/CaMnO_3$. The XPS system used a Thermo-Fisher Alpha 110 hemispherical energy analyzer and XR3 300 W dual-anode X-ray source, and samples were excited using an Al anode (1486.7 eV). Data processing and analysis were performed in the CasaXPS program (Casa Software Ltd., U.K.). All binding energies were calibrated to the adventitious C 1s peak at 284.6 eV, and narrow scans were processed with a 21-point smoothing function. Peak areas for the metal atoms were normalized by their relative sensitivity factors to C 1s in CasaXPS and totaled in order to calculate surface atomic percentages; this calculation was done on a carbon- and oxygen-free basis.

Co-feed H_2/C_2H_4 TPR (temperature-programmed reaction) was used to screen the SHC properties of the redox catalysts. TPR experiments were carried out over 100 mg of redox catalyst loaded in a fixed-bed quartz U-tube reactor; further details on the reactor configuration are given in the second section. Prior to TPR runs, catalyst samples were heated to 900°C, held there for 30 min, and allowed to cool, all under 10% O_2 in Ar (100 mL/min total). The redox catalysts were then heated from 350 to 850°C at a ramping rate of 5°C/min under 100 mL/min (H_2:C_2H_4 = 2.5%:2.5% v/v in Ar). Products formed during TPR runs were analyzed by a quadrupole mass spectrometer (MKS Cirrus II). H_2O peaks and CO/CO_2 (CO_x) signals were analyzed to quantify oxidation of H_2 and C_2H_4, respectively; in most cases, CO_x signals were negligible. CO was calculated from mass 28 by subtracting contributions by CO_2 and C_2H_4 using characteristic ratios of 44/28 and 26/28 determined from three-point MS calibrations.

Reaction testing

To evaluate SHC properties in a simulated CL-ODH setting, isothermal redox cycling experiments were carried out in a fixed-bed quartz microtubular reactor (ID = 1/8 in.) at atmospheric pressure. Quartz wool was placed on either side of a 0.1 g bed of redox catalyst (sized 250–425 μm). Aluminum oxide grit (16 mesh) filled the remaining void space to limit gas volume in the heated zone of the reactor. The reactor tube was secured in a tube furnace a K-type thermocouple and a temperature controller. Inlet gas flow rate and composition were set with a panel of valves and mass flow controllers, and the redox cycles were implemented with an automated valve switching program.

Prior to any TPR or redox cycling experiments, samples were pre-treated with six ethane ODH redox cycles, three at 900°C followed by three at 850°C. During the reduction step, 60 mL/min C_2H_6 and 15 mL/min Ar were flowed for 3 min, followed by a 75 mL/min Ar purge for 5 min, then a regeneration step at 75 mL/min Ar and 15 mL/min O_2 for 3 min, and finally another 75 mL/min Ar purge for 5 min. A second type of redox cycle was used to evaluate SHC properties of the redox catalysts by simulating the product composition from ethane dehydrogenation.[35,36] The reduction step consisted of 40%:40% H_2:C_2H_4 v/v in Ar at 100 mL/min total. This reducing mixture flowed for 10 s to create a reducing gas volume of 13.3 mL. 17% O_2 v/v in Ar was subsequently flowed at 120 mL/min for 3 min to re-oxidize the sample. Between each step, Ar was flowed for 5 min at 100 mL/min. Using a manual valve switch, effluent gas from the reducing step was flowed into a sample bag for quantitative analysis via GC. At each temperature, two redox cycles were completed first before the effluent was sampled.

Gas chromatography (GC, Agilent Technologies 7890B) was used to analyze the outlet gas from the reactor. A flame ionization detector channel identified and quantified hydrocarbons, while Ar and He thermal conductivity detectors identified H_2 and CO_x gases, respectively. GC signals were calibrated using a refinery-grade gas standard, and volume percentages were calculated by integrating signal peaks. An atomic C balance was used to determine ethylene conversion as well as yields of all observed hydrocarbons; carbon losses to coking were determined to be less than 2% for all cycle experiments. H_2O formation during the reduction step was calculated based on an atomic H balance, which was then used to calculate molar conversion of H_2 and C_2H_4 by combustion reactions, and SHC selectivity, defined as (H_2 conversion)/(H_2 + C_2H_4 conversion). H_2 formed as a byproduct of C_2H_4 combustion was not included in calculating H_2 conversion. All cycles not analyzed with GC were sent downstream to the mass spectrometer (MS) for confirmation of GC results and for quantification of coke formation.

Results and Discussion

Structure characterization

All six redox catalysts investigated in this study were characterized via X-ray powder diffraction (XRD) to confirm the presence of expected phases. Figure 2 shows the XRD patterns for the as-prepared samples. Structural matches were obtained for Mg_6MnO_8 (ICDD PDF# 01–074-1903), $SrMnO_3$ (PDF#

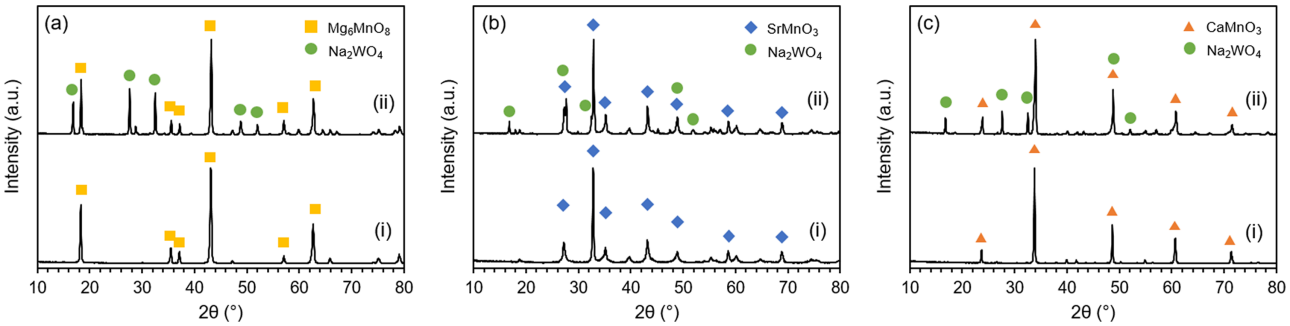

Figure 2. XRD patterns for (a) Mg_6MnO_8 (i) and 20 wt % Na_2WO_4/Mg_6MnO_8 (ii); (b) $SrMnO_3$ (i) and 20 wt % $Na_2WO_4/SrMnO_3$ (ii); and (c) $CaMnO_3$ (i) and 20 wt % $Na_2WO_4/CaMnO_3$ (ii).

[Color figure can be viewed at wileyonlinelibrary.com]

00-024-1213), and $CaMnO_3$ (PDF# 04-016-1860). Sodium tungstate manifested in a crystalline phase for each material promoted with 20 wt % Na_2WO_4 (PDF# 04-008-8508). All of the redox catalysts exhibited low surface area (<10 m^2/g) as determined by BET analysis, and Na_2WO_4 promotion further lowered the surface areas (Table 1).

Material screening

The primary function of the redox catalysts is to enhance ethylene or propylene yields from dehydrogenation reactions via selective hydrogen combustion. Throughout this work, ethane to ethylene/H_2 was used as the model reaction. Prior to reactivity testing in a cyclic redox reaction, TPR experiments were conducted to screen the materials and determine temperature ranges at which these materials facilitated SHC.

The reducibility of the redox catalysts is illustrated in Figure 3. In all cases, reduction of the metal oxide by C_2H_4, which can be quantified by CO_x areas, was found to be insignificant (less than 5% of total peak area, including H_2O). Therefore, only the H_2O signal (m/z = 18) is shown here, with complete MS signal data (H_2, C_2H_4, CO, CO_2) relegated to Figures S1–S6. Figure 3a shows the oxygen release behavior of the Mg_6MnO_8 system with and without Na_2WO_4. The unpromoted Mg_6MnO_8 was active for H_2 combustion at as low as 550°C. In comparison to the unpromoted sample, Mg_6MnO_8 promoted with 20 wt % Na_2WO_4 behaved significantly differently (Figure 3a), in general agreement with previous literature.[20] With Na_2WO_4 promotion, Mg_6MnO_8 showed notable hydrogen combustion activity only at 750°C and above. We note that gas phase reactions also became significant at 750°C and above, with C_2H_4 conversion $\geq$3%. However, no CO_x formation was observed, a result later supported by isothermal redox cycling at these temperatures.

Figure 3b shows the reducibility of the $SrMnO_3$ system. $SrMnO_3$ became active for H_2 combustion around 450°C, peaking around 590°C, and exhibited slower oxygen release compared to Mg_6MnO_8, apparent from the wider H_2O peak.

Table 1. BET Surface Areas (S_{BET}, m^2/g) for As-Prepared Redox Catalysts

Redox Catalyst	S_{BET} (m^2/g)
Mg_6MnO_8	7.3
Na_2WO_4/Mg_6MnO_8	2.7
$SrMnO_3$	6.8
$Na_2WO_4/SrMnO_3$	3.1
$CaMnO_3$	2.2
$Na_2WO_4/CaMnO_3$	2.0

Upon promotion with Na_2WO_4, the material became less reducible, and H_2O did not appear until 605°C, peaking near 685°C. The presence of Na_2WO_4 had two effects: it increased the initial reduction temperature but leads to a more narrow peak at a higher temperature. Figure 3c demonstrates the effect of Na_2WO_4 on the reduction of the $CaMnO_3$ system. The bulk material exhibited similar behavior to bulk $SrMnO_3$, including a wide temperature range for H_2 combustion and a peak appearing around 600°C. However, the H_2O peak had a shoulder extending to 665°C, possibly indicating phase change during the reduction reaction. Promotion $CaMnO_3$ with Na_2WO_4 altered the H_2 combustion properties significantly; reduction did not occur until 620°C, and the peak for H_2O shifted to 705°C.

Table 2 summarizes the peak temperatures for all samples. Addition of Na_2WO_4 increased the initial reduction and peak temperatures for H_2 combustion. The effect of Na_2WO_4 was similar for the two perovskite materials, i.e., addition of Na_2WO_4 increased the peak temperature by 85–95°C. In comparison, Na_2WO_4 suppressed the SHC activity for the rock salt structured Mg_6MnO_8 in a much more significant manner, with a more than 235°C increase in the peak temperature. Moreover, four of the catalysts exhibited sharp reduction peaks with the following order: $Mg_6MnO_8 < Na_2WO_4/SrMnO_3 < Na_2WO_4/CaMnO_3 < Na_2WO_4/Mg_6MnO_8$. This indicates that the SHC properties of redox catalysts can potentially be adjusted by careful selection of substrate and promoter. The main body of cyclic redox-mode reactivity testing presented in the remainder of this study was designed to validate the possibility of tuning SHC properties (i.e., H_2 conversion and SHC selectivity) for the redox catalysts.

SHC properties of redox catalysts

Cycling at isothermal conditions can better represent typical CL-ODH operating modes. As such, a series of redox experiments was carried out to assess the SHC properties of the six redox catalysts within the temperature range 550–850°C. This temperature range was selected based on the TPR results shown in Figure 3. Equimolar H_2 and C_2H_4 was fed to the reactor in 10-s step injections at a flowrate of 100 cm^3 STP/min, as described in the second section. The reactions included combustion of H_2 to H_2O and combustion of C_2H_4 to CO and CO_2, though gas phase reactions can occur at high temperatures. Reaction testing results for the six redox catalysts are presented in Figure 4. Estimated oxygen release or oxygen carrying capacity (in wt %) from each redox catalyst as a function of temperature, calculated based on material balance

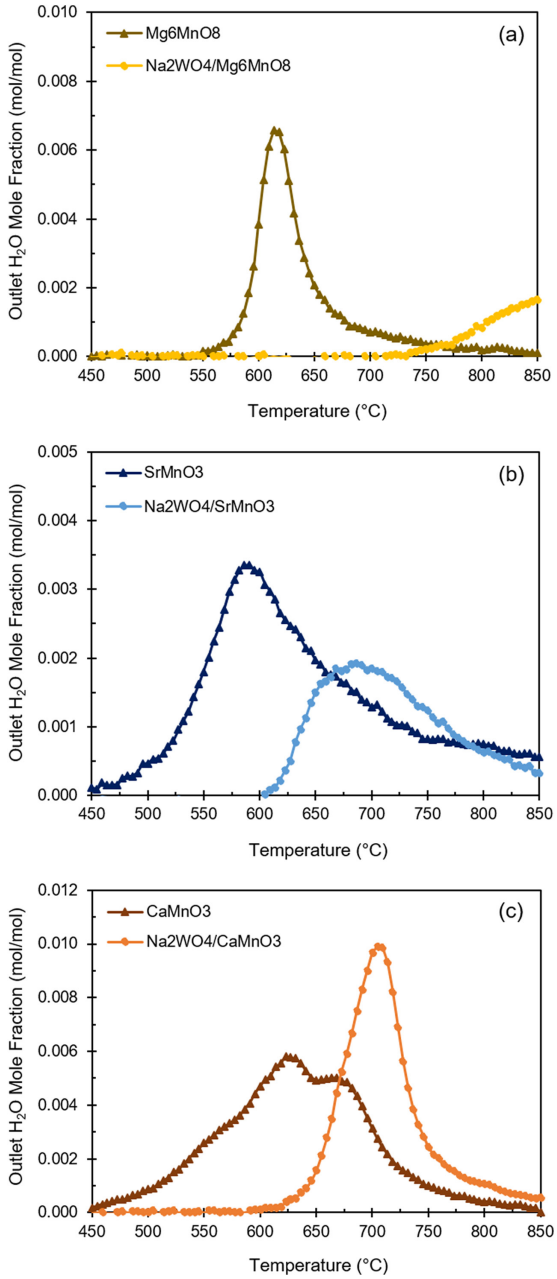

Figure 3. H_2O generation based on MS signal (m/z = 18) during H_2/C_2H_4 TPR for the three redox catalyst systems: (a) Mg_6MnO_8; (b) $SrMnO_3$; and (c) $CaMnO_3$. Conditions: $m = 100$ mg, $F = 100$ ml/min, $H_2:C_2H_4 = 2.5\%:2.5\%$ v/v in Ar, ramping rate = 5°C/min.

[Color figure can be viewed at wileyonlinelibrary.com]

across the experiments shown in Figure 4, are included in Figures S7–S9.

Figure 4a illustrates the SHC performance of the Mg_6MnO_8 redox catalyst system. As previously observed in the TPR screening experiments, Mg_6MnO_8 activates hydrogen gas beginning around 550°C and exhibits ~20% oxidative conversion of H_2 at 550°C. The peak of H_2 conversion occurs around 650°C, after which the observed oxidation of H_2 begins to decline as a result of decreasing SHC selectivity—the relative rate of hydrogen combustion decreases, while that of ethylene combustion increases. At 850°C, unpromoted Mg_6MnO_8 shows an SHC selectivity of 60%. Addition of sodium tungstate results in a significant change in SHC properties. Na_2WO_4-promoted Mg_6MnO_8 does not exhibit significant activity (i.e., achieve greater than 5% H_2 conversion) until 800°C, in agreement with TPR results, and at 850°C the activity is approximately 20% toward H_2 conversion. This is comparable to the activity of Mg_6MnO_8 at the same temperature, but Na_2WO_4 increases the selectivity to hydrogen combustion by more than 30% to a total SHC selectivity of 96%. This is the highest SHC selectivity of all six materials examined herein at 850°C.

Results from isothermal cycling on the $SrMnO_3$ redox catalyst system are shown in Figure 4b. It is apparent that materials based on $SrMnO_3$ are suitable for selective hydrogen combustion over much of the tested temperature range; both $SrMnO_3$ and 20 wt % Na_2WO_4-promoted $SrMnO_3$ show over 90% SHC selectivity up to 825°C even as the activity toward hydrogen conversion is 50% or greater. Significant and selective activation of hydrogen is seen at 550°C for both materials, and this conversion remains selective at higher temperatures, indicating that $SrMnO_3$ is an effective redox catalyst for SHC around 700°C. Most notably, a significant difference between the Mg_6MnO_8 system and the $SrMnO_3$ system is the lack of significant effect of the Na_2WO_4 promoter in the latter material. The increase in SHC selectivity by adding Na_2WO_4 to the base material is countered by a marked decrease (15–20%) in overall H_2 conversion.

Figure 4c shows cycling results for the $CaMnO_3$ system of redox catalysts. Both unpromoted and Na_2WO_4-promoted $CaMnO_3$ are active in the upper region of the tested temperature range (~700°C and greater). This is in agreement with screening results from TPR experiments in which the H_2 oxidation peaks manifested at an average of 650 and 700°C for the bulk and promoted sample, respectively. The effect of promotion is more evident for this perovskite than for $SrMnO_3$ in terms of the selectivity increase. Sodium tungstate impregnation results in an only marginally less active material (the greatest difference in H_2 conversion between materials is approximately 15% at 750°C); however, the Na_2WO_4-promoted sample is much more selective toward hydrogen combustion (SHC selectivity increases by 5% at 850°C with equal H_2 conversion). Generally, the $CaMnO_3$-based materials are the most suitable for hydrogen combustion out of the materials examined in this study, particularly in terms of oxygen capacity. However, neither the $CaMnO_3$ nor Na_2WO_4-promoted $CaMnO_3$ converts as much H_2 as the $SrMnO_3$ materials at temperatures below 750°C. At temperatures near 850°C, Na_2WO_4-promoted Mg_6MnO_8 becomes a more desirable material for SHC due to its greater selectivity. Therefore, the utility of $Na_2WO_4/CaMnO_3$ for SHC lies between these two aforementioned materials, at temperatures from about 750–

Table 2. Reduction Onset Temperatures (T_o) and Peak Temperatures (T_p) over Redox Catalysts as Determined by H_2/C_2H_4 TPR

Redox Catalyst	T_o (°C)	T_p (°C)
Mg_6MnO_8	545	615
Na_2WO_4/Mg_6MnO_8	740	>850
$SrMnO_3$	450	590
$Na_2WO_4/SrMnO_3$	605	685
$CaMnO_3$	435	620; 665
$Na_2WO_4/CaMnO_3$	620	705

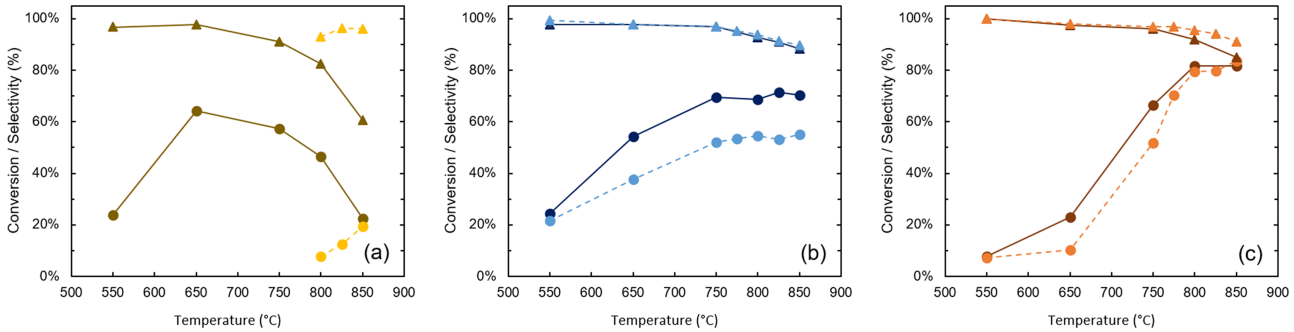

Figure 4. Hydrogen conversion (●) and selectivity toward hydrogen combustion (▲) for the unpromoted (—) and Na_2WO_4-promoted (– –) redox catalysts: (a) Mg_6MnO_8; (b) $SrMnO_3$; (c) $CaMnO_3$. Conversion and selectivity are determined via C and H atomic balances from GC analysis of entire step volumes. Conditions: m = 100 mg, F = 100 mL/min, H_2:C_2H_4 = 40%:40% v/v in Ar, step duration = 10 s.

[Color figure can be viewed at wileyonlinelibrary.com]

850°C. Promotion with Na_2WO_4 enables selective H_2 combustion at temperatures slightly higher than bulk $CaMnO_3$ is capable of (up to 800°C).

Figures 4a–c show several trends. First, SHC is facile at low temperatures (650°C), where five of the six materials (excluding Na_2WO_4/Mg_6MnO_8) achieve a molar hydrogen combustion selectivity of 97% or greater. As indicated in the figures, the apparent activation energy for hydrogen combustion is significantly lower than that for ethylene combustion. Second, the addition of sodium tungstate via wet impregnation has the consistent effect of suppressing oxygen donation from the redox catalysts, which manifests as (i) higher reduction peak temperatures and active ranges, (ii) decreased activity at identical temperatures compared to unpromoted materials, and (iii) greater selectivity toward hydrogen combustion. This effect is far more pronounced for the Mg_6MnO_8 system. Third, while the selectivity toward hydrogen combustion and the magnitude of the combustion activity are inversely related, high values for H_2 combustion (greater than 70%) may still be realized while maintaining an SHC selectivity of 90% or greater, as evidenced by the Na_2WO_4-promoted $CaMnO_3$ data. This is beneficial for a cyclic ethane ODH scheme; a previous simulation study on the topic indicated that 71% H_2 combustion by an oxygen carrier was ideal for obtaining high ethylene yields.[7] This relationship between activity and selectivity is highly dependent on the metal oxide substrate.

It is evident that the three redox catalyst systems in this study can be selective for hydrogen combustion via lattice oxygen donation at varying temperature ranges. Moreover, the addition of sodium tungstate increases the SHC selectivity in all cases. One can therefore envision that SHC materials may be designed via a combination of a metal oxide substrate and an alkali tungstate promoter to meet specific operating temperature ranges of a process application. As an example, an ethane ODH reactor operated at 850°C and a residence time of 0.1 s with 70% ethane conversion would require approximately 71% in-situ combustion of H_2 from a process heat balance standpoint.[7] This corresponds to an H_2 combustion rate of 39.4 mmol H_2 per kg catalyst per second. A similar specific combustion "rate" can be derived from the experimental GC results of this study by calculating a time-averaged combustion rate of H_2, taking into account the feed flowrates and bed mass. Figure 5 thus presents the SHC properties of the six redox catalysts by temperature, using a threshold of 40 mmol H_2/kg-cat·s to represent a useful H_2 combustion activity, along with a selectivity toward SHC of 95% or higher.

Gas hourly space velocity (GHSV, h^{-1}) is an important process condition to consider. Typical ethane steam cracking units operate at a GHSV range of 1800–8000 h^{-1} STP.[2,11] Figure 6 illustrates the effect of changing space velocity with the relatively less active Na_2WO_4/Mg_6MnO_8 redox catalyst (Figure 6a) and the more active $Na_2WO_4/CaMnO_3$ redox catalyst (Figure 6b). The change in space velocity results in more moderate levels of hydrogen combustion without any loss in SHC selectivity for either redox catalyst. Interestingly, the decrease in fractional H_2 conversion for $Na_2WO_4/CaMnO_3$ was minimal (less than 10%) even when space velocity and total H_2 volume was increased by 50%, indicating that the material has both a large oxygen capacity and fast kinetics. Along with

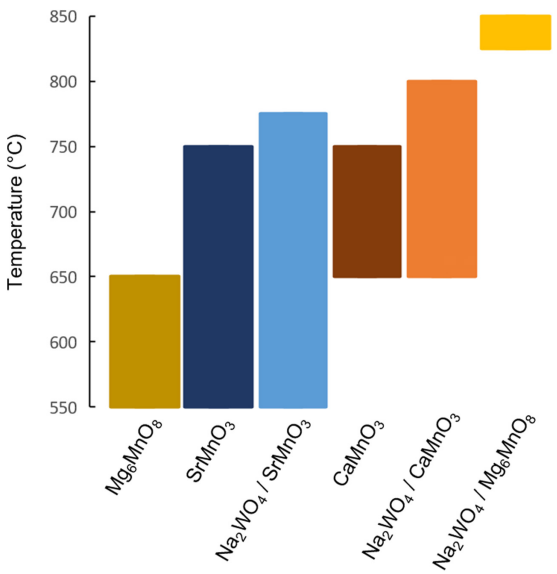

Figure 5. Selective hydrogen combustion (SHC) properties of the six redox catalyst materials.

Each bar represents the temperature range within which the catalyst provides an H_2 conversion rate of at least 40 mmol H_2/kg-cat·s (averaged over a 10 s step) and at least 95% SHC selectivity. By varying the metal oxide substrate and by promotion with Na_2WO_4, a wide range of operating temperatures is covered. [Color figure can be viewed at wileyonlinelibrary.com]

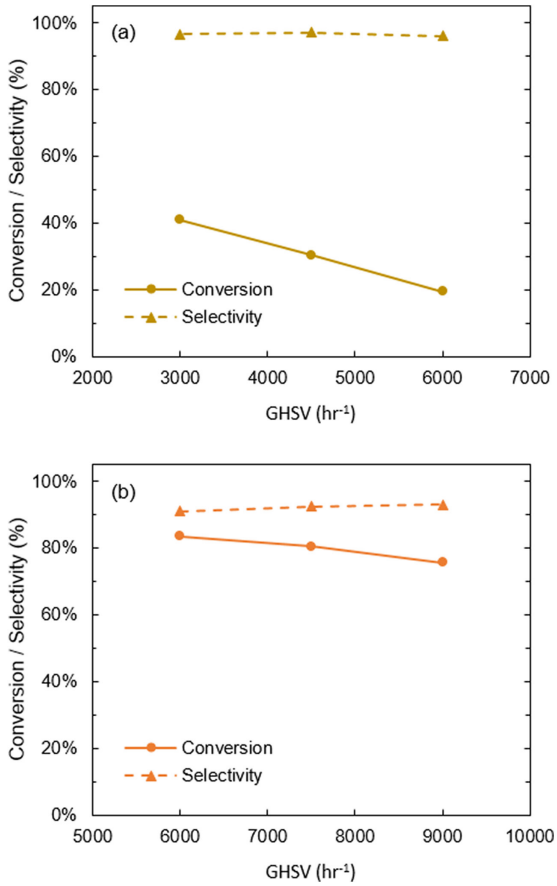

Figure 6. Effect of altering gas hourly space velocity (GHSV) through the reactor on molar H_2 conversion and SHC selectivity; (a) lower GHSV over Na_2WO_4/Mg_6MnO_8, and; (b) higher GHSV over $Na_2WO_4/CaMnO_3$. GHSV = 6000 h^{-1} corresponds to $\tau \approx 0.15$ s. Conditions: $m = 100$ mg, H_2:C_2H_4 = 40%:40% v/v in Ar, step duration = 10 s, $T = 850°C$.

[Color figure can be viewed at wileyonlinelibrary.com]

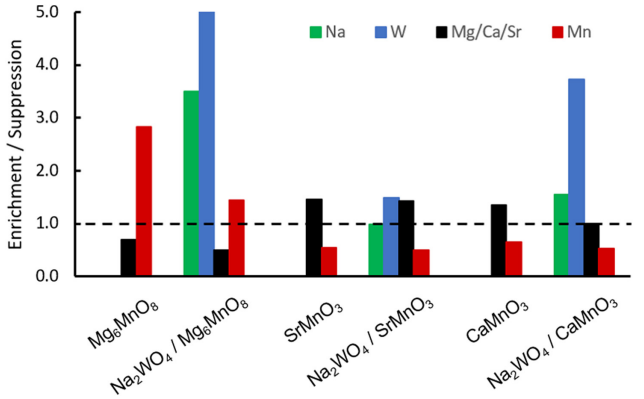

Figure 7. Near-surface enrichment (>1) and suppression (<1) ratios of metal atoms in asprepared catalysts, determined via XPS narrow scan analysis.

Enrichment and suppression are calculated based on the bulk atomic composition expected from the material stoichiometry. [Color figure can be viewed at wileyonlinelibrary.com]

operating temperature, gas contact time or feed flowrate requirements should be included in the design parameters for the SHC redox catalysts.

With the goal of correlating redox catalyst SHC properties to near-surface atomic composition, we obtained X-ray photoelectron spectra (XPS) for each of the six redox catalysts investigated. Near-surface atomic percentages were calculated using the total of the corrected areas for each metal spectrum. Results of near-surface composition analysis are presented in Table 3. From the observed atomic percentages, an enrichment or suppression for each metal cation was derived based on the average atomic composition of the bulk material. Figure 7 presents these enrichment (greater than 1) and suppression (less than 1) ratios for the redox catalysts.

Atomic percentages and enrichment behavior obtained for the Mg_6MnO_8 system are in good agreement with the XPS results reported by Yusuf et al.[22] In particular, manganese content in the near-surface of Mg_6MnO_8 is greater than the bulk formulation ratio of Mg/Mn; Mn exhibits an enrichment of 2.84. Upon promotion by Na_2WO_4, near-surface manganese is suppressed significantly. Moreover, sodium (25.0 at%, 3.50) and tungsten (17.9 at%, 5.01) are present in such quantities as to suggest enrichment of Na_2WO_4 on the surface. These results together with cycling data suggest that this surface enrichment is at least in part responsible for the selectivity of the catalyst toward hydrogen combustion.[22] To date, the effect of Na_2WO_4 promotion on the near-surface composition of perovskite oxide structures has not been studied. As seen in Figure 7, the Na (0.98) and W (1.49) near-surface enrichment on promoted $SrMnO_3$ is only slight, and Mn suppression is also insignificant. In conjunction with reaction data, these results suggest that Na_2WO_4 does not create a radically different near-surface environment from the unpromoted formulation of $SrMnO_3$. These surface composition results are consistent with experimental findings that Na_2WO_4 promotion does not significantly change the SHC properties of the $SrMnO_3$ redox catalyst.

In the $CaMnO_3$ system, a greater degree of Na and W enrichment (Na = 1.56, W = 3.73) is seen than in the $SrMnO_3$ system, along with slightly more significant Mn suppression. This correlates with more noticeably altered SHC behavior between the bulk and Na_2WO_4-promoted samples of this

Table 3. Near-Surface Atomic Percentages of Metal Cations on Fresh and Cycled Redox Catalysts, Obtained via XPS (on an Oxygen- and Carbon-Free Basis): Dashes Indicate No Measurement was Taken

Redox Catalyst	Mg 2s (%)	Sr 3d (%)	Ca 2p (%)	Mn 2p (%)	Na 1s (%)	W 4f (%)
Mg_6MnO_8	59.5	–	–	40.5	0.0	0.0
Na_2WO_4/Mg_6MnO_8	38.8	–	–	18.4	25.0	17.9
$SrMnO_3$	–	73.0	–	27.0	0.0	0.0
$Na_2WO_4/SrMnO_3$	–	57.5	–	19.9	12.8	9.7
$CaMnO_3$	–	–	67.5	32.5	0.0	0.0
$Na_2WO_4/CaMnO_3$	–	–	42.2	22.6	16.0	19.2

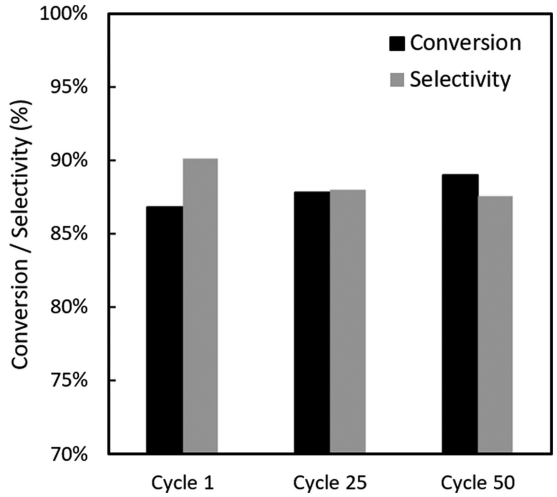

Figure 8. Redox cycling stability of the 20 wt % Na2WO4/CaMnO3 redox catalyst over 50 cycles.

Conversion and selectivity were calculated via C and H atomic balances of GC data. Conditions: m = 100 mg, F = 100 ml/min, H_2:C_2H_4 = 40%:40% v/v in Ar, step duration = 10 s, T = 850°C.

system; promoted $CaMnO_3$ retains its selectivity toward SHC at higher temperature (~800°C). It can be surmised from these data and from the effects of Na_2WO_4 promotion in the Mg_6MnO_8 system that Na and W enrichment on the material surfaces is related to high-temperature SHC capability. Both Sr and Ca are enriched relative to Mn in the near-surface for their respective perovskite oxides, regardless of promoter content; this Mn suppression may create a suitable structure for SHC activity by $SrMnO_3$ and $CaMnO_3$. Another noteworthy feature of the XPS data is a relative enrichment of W compared to Na in the promoted materials.

Long-term stability and application in ethane dehydrogenation

To obtain further understanding of the effects of redox cycles on the SHC-active redox catalysts and particularly on the Na_2WO_4 promoter, the promoted $CaMnO_3$ redox catalyst was cycled 50 times. A high operating temperature of 850°C was selected to investigate the stability of the redox catalyst. As can be seen in Figure 8, the SHC properties of the $Na_2WO_4/CaMnO_3$ redox catalyst were stable, with slight decrease in SHC selectivity and increase in activity over 50 cycles. These results indicate that Na_2WO_4-promoted $CaMnO_3$ can be suitable for SHC under continuous redox cycles in a CL-ODH scheme.

In combination with cracking or dehydrogenation, redox catalysts possessing SHC properties can selectively oxidize the H_2 co-product. In the case of dehydrogenation with selective hydrogen combustion (DH + SHC), the redox catalyst for SHC can be loaded either in series with, or as part of a physical mixture with, a catalytic dehydrogenation catalyst.[30,31] The latter approach was adopted in this study to demonstrate the SHC properties of 20 wt % $Na_2WO_4/CaMnO_3$ in series with Cr_2O_3/Al_2O_3, an ethane dehydrogenation catalyst.

The results of a single-bed ethane dehydrogenation experiment (250 mg Cr_2O_3/Al_2O_3) and a sequential bed DH + SHC experiment (150 mg Cr_2O_3/Al_2O_3 followed by 500 mg $Na_2WO_4/CaMnO_3$) at 650°C are presented in Figure 9. Consistent with previous SHC experiments with this redox catalyst, the $Na_2WO_4/CaMnO_3$ selectively combusted over 84% of the H_2 co-product. CO_x yield was less than 2% and C_2H_4 yield was unchanged from the Cr_2O_3/Al_2O_3 single bed experiment (approximately 45% at 650°C after 30 min). These preliminary results demonstrate that redox catalysts for SHC such as those developed in this study can be combined with catalytic dehydrogenation catalysts to facilitate the selective combustion of hydrogen under a CL-ODH scheme.

Conclusion

Six Mn-containing redox catalysts were investigated and found to exhibit varying selective hydrogen combustion properties across the temperature range of 550–850°C. Generally, H_2 conversion increased and SHC selectivity decreased at higher temperatures. Without a promoter, the base materials were capable of SHC in different temperature ranges, increasing in the order $Mg_6MnO_8 < SrMnO_3 < CaMnO_3$. Promotion by Na_2WO_4 increased the SHC selectivity of the mixed oxides

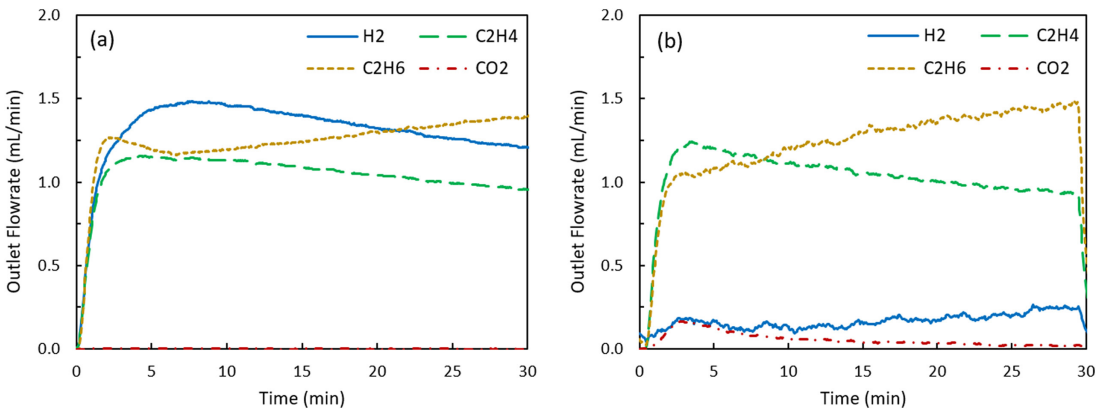

Figure 9. Sequential bed results for Cr_2O_3/Al_2O_3 (ethane dehydrogenation) followed by $Na_2WO_4/CaMnO_3$ redox catalyst (selective hydrogen combustion).

(a) Results of single Cr_2O_3/Al_2O_3 bed showing ethane dehydrogenation; (b) Sequential bed with $Na_2WO_4/CaMnO_3$. The redox catalyst consumes 84% of H_2 generated by ethane dehydrogenation. Conditions: m_{EDH} = 250 mg (a) or 150 mg (b), m_{SHC} = 500 mg, F = 50 mL/min, 5% C_2H_6 v/v in Ar, T = 650°C. [Color figure can be viewed at wileyonlinelibrary.com]

but suppressed the H_2 combustion activity; this effect was most significant on the Na_2WO_4-promoted Mg_6MnO_8, which was found to be the only redox catalyst suitable for SHC above 800°C. The selectivity enhancement effect of Na_2WO_4 promotion was also significant for the $CaMnO_3$ redox catalyst. XPS analysis of the redox catalysts indicated that SHC selectivity was inversely related to the surface Mn content. Addition of the Na_2WO_4 promoter led to varying degrees of Mn suppression near the surface; promoted Mg_6MnO_8 exhibited significant Na and W enrichment which was positively correlated with SHC selectivity results obtained from cyclic reaction testing. Na_2WO_4-promoted $CaMnO_3$ showed stable SHC performance over 50 redox cycles. When placed downstream of an ethane dehydrogenation catalyst bed, this redox catalyst is suitable for selective hydrogen combustion with over 84% hydrogen conversion and less than 2% CO_x yield.

Acknowledgments

This work was supported by the U.S. National Science Foundation (Award No. CBET-1604605) and the Kenan Institute for Engineering, Technology and Science at NC State University. The authors acknowledge the use of the Analytical Instrumentation Facility (AIF) at North Carolina State University, which is supported by the State of North Carolina and the National Science Foundation. The authors would also like to acknowledge the assistance for XPS measurements from Prof. Fang He and Dr. Kun Zhao at Guangzhou Institute of Energy Conversion, Chinese Academy of Sciences.

Literature Cited

1. International Energy Agency. *Technology Roadmap: Energy and GHG Reductions in the Chemical Industry via Catalytic Processes*. Paris, France: IEA Publications, 2013.
2. Zimmermann H, Walzl R. Ethylene. In: Elvers B., editor, *Ullmann's Encyclopedia of Industrial Chemistry*. Weinheim, Germany: Wiley-VCH, 2012:547–572.
3. Zimmermann H. Propene. In: Elvers B., editor, *Ullmann's Encyclopedia of Industrial Chemistry*, *Vol*. 6. Weinheim, Germany: Wiley-VCH, 2014:45–66.
4. Ren T, Patel M, Blok K. Olefins from conventional and heavy feedstocks: energy use in steam cracking and alternative processes. *Energy*. 2006;31(4):425–451. doi:10.1016/j.energy.2005.04.001.
5. Bhasin MM, McCain JH, Vora BV, Imai T, Pujadó PR. Dehydrogenation and oxydehydrogenation of paraffins to olefins. *Appl Catal A Gen*. 2001;221(1–2):397–419. doi:10.1016/S0926-860X(01)00816-X.
6. Sattler JJHB, Ruiz-Martinez J, Santillan-Jimenez E, Weckhuysen BM. Catalytic dehydrogenation of light alkanes on metals and metal oxides. *Chem Rev*. 2014;114(20):10613–10653. doi:10.1021/cr5002436.
7. Haribal VP, Neal LM, Li F. Oxidative dehydrogenation of ethane under a cyclic redox scheme: process simulation and analysis. *Energy*. 2017;119:1024–1035. doi:10.1016/j.energy.2016.11.039.
8. Mamedov EA, Cortes CV. Oxidative dehydrogenation of lower alkanes on vanadium oxide-based catalysts. The present state of the art and outlooks. *Appl Catal A Gen*. 1995;127(1–2):1–40. doi:10.1016/0926-860X(95)00056-9.
9. Cavani F, Trifirò F. The oxidative dehydrogenation of ethane and propane as an alternative way for the production of light olefins. *Catal Today*. 1995;24(3):307–313. doi:10.1016/0920-5861(95)00051-G.
10. Cavani F, Ballarini N, Cericola A. Oxidative dehydrogenation of ethane and propane: How far from commercial implementation? *Catal Today*. 2007;127(1–4):113–131. doi:10.1016/j.cattod.2007.05.009.
11. Gärtner CA, van Veen AC, Lercher JA. Oxidative dehydrogenation of ethane: common principles and mechanistic aspects. *ChemCatChem*. 2013;5(11):3196–3217. doi:10.1002/cctc.201200966.
12. Blasco T, Lopez-Nieto JM. Oxidative dyhydrogenation of short chain alkanes on supported vanadium oxide catalysts. *Appl Catal A Gen*. 1997;157(1–2):117–142. doi:10.1016/S0926-860X(97)00029-X.
13. Stern DL, Grasselli RK. Propane oxydehydrogenation over molybdate-based catalysts. *J Catal*. 1997;167(2):550–559. doi:10.1006/jcat.1997.1568.
14. Grabowski R, Grzybowska B, Samson K, Słoczyński J, Stoch J, Wcisło K. Effect of alkaline promoters on catalytic activity of V_2O_5 TiO_2 and MoO_3 TiO_2 catalysts in oxidative dehydrogenation of propane and in isopropanol decomposition. *Appl Catal A Gen Gen*. 1995;125(1):129–144.
15. Chen K, Bell AT, Iglesia E. Kinetics and mechanism of oxidative dehydrogenation of propane on vanadium, molybdenum, and tungsten oxides. *J Phys Chem B*. 2000;104(6):1292–1299.
16. Chen K, Xie S, Bell AT, Iglesia E. Alkali effects on molybdenum oxide catalysts for the oxidative dehydrogenation of propane. *J Catal*. 2000;195(2):244–252. doi:10.1006/jcat.2000.3025.
17. Huff M, Schmidt LD. Ethylene formation by oxidative dehydrogenation of ethane over monoliths at very short contact times. *J Phys Chem*. 1993;97(45):11815–11822. doi:10.1021/j100147a040.
18. Huff M, Schmidt LD. Production of olefins by oxidative dehydrogenation of propane and butane over monoliths at short contact times. *J Catal*. 1994;149(1):127–141.
19. Ballarini N, Cavani F, Cericola A, Cortelli C, Ferrari M, Trifirò F, Capannelli G, Comite A, Catani R, Cornaro U. Supported vanadium oxide-based catalysts for the oxidehydrogenation of propane under cyclic conditions. *Catal Today*. 2004;91–92:99–104. doi:10.1016/j.cattod.2004.03.016.
20. Neal LM, Yusuf S, Sofranko JA, Li F. Oxidative dehydrogenation of ethane: a chemical looping approach. *Energy Technol*. 2016;4(10):1200–1208. doi:10.1002/ente.201600074.
21. Gao Y, Neal LM, Li F. Li-promoted $La_xSr_{2-x}FeO_{4-d}$ core-shell redox catalysts for oxidative dehydrogenation of ethane under a cyclic redox scheme. *ACS Catal*. 2016;6(11):7293–7302. doi:10.1021/acscatal.6b01399.
22. Yusuf S, Neal LM, Li F. Effect of promoters on manganese-containing mixed metal oxides for oxidative dehydrogenation of ethane via a cyclic redox scheme. *ACS Catal*. 2017;7(8):5163–5173. doi:10.1021/acscatal.7b02004.
23. Li F, Fan L-S. Clean coal conversion processes—progress and challenges. *Energy Environ Sci*. 2008;1(2):248. doi:10.1039/b809218b.
24. Fan L-S. *Chemical Looping Systems for Fossil Energy Conversions*. Hoboken, NJ: John Wiley & Sons, Inc., 2010.
25. Adanez J, Abad A, Garcia-Labiano F, Gayan P, De Diego LF. Progress in chemical-looping combustion and reforming technologies. *Prog Energy Combust Sci*. 2012;38(2):215–282. doi:10.1016/j.pecs.2011.09.001.
26. Al-Ghamdi S, Volpe M, Hossain MM, Lasa HD. VOx/c-Al_2O_3 catalyst for oxidative dehydrogenation of ethane to ethylene: desorption kinetics and catalytic activity. *Appl Catal A Gen*. 2013;450:120–130. doi:10.1016/j.apcata.2012.10.007.
27. Al-Ghamdi SA, Lasa HID. Propylene production via propane oxidative dehydrogenation over VOx/c-Al_2O_3 catalyst. *Fuel*. 2014;128:120–140. doi:10.1016/j.fuel.2014.02.033.
28. Bakare IA, Mohamed SA, Al-Ghamdi S, Razzak SA, Hossain MM, Lasa HID. Fluidized bed ODH of ethane to ethylene over VOx-MoO_x/Al_2O_3 catalyst: desorption kinetics and catalytic activity. *Chem Eng J*. 2015;278:207–216. doi:10.1016/j.cej.2014.09.114.
29. Elbadawi AH, Ba-Shammakh MS, Al-Ghamdi S, Razzak SA, Hossain MM. Reduction kinetics and catalytic activity of VOx/Al_2O_3-ZrO_2 for gas phase oxygen free ODH of ethane. *Chem Eng J*. 2016;284:448–457. doi:10.1016/j.cej.2015.08.048.
30. Grasselli RK, Stern DL, Tsikoyiannis JG. Catalytic dehydrogenation (DH) of light paraffins combined with selective hydrogen combustion (SHC) I. DH -> SHC -> DH catalysts in series (co-fed process mode). *Appl Catal A Gen*. 1999;189(1):1–8. doi:10.1016/S0926-860X(99)00224-0.
31. Grasselli RK, Stern DL, Tsikoyiannis JG. Catalytic dehydrogenation (DH) of light paraffins combined with selective hydrogen combustion (SHC) II. DH+SHC catalysts physically mixed (redox process mode). *Appl Catal A Gen*. 1999;189(1):9–14. doi:10.1016/S0926-860X(99)00224-0.
32. Tsikoyiannis JG, Stern DL, Grasselli RK. Metal oxides as selective hydrogen combustion (SHC) catalysts and their potential in light paraffin dehydrogenation. *J Catal*. 1999;184(1):77–86. doi:10.1006/jcat.1998.2363.
33. Låte L, Rundereim JI, Blekkan EA. Selective combustion of hydrogen in the presence of hydrocarbons: 1. Pt-based catalysts. *Appl Catal A Gen*. 2004;262(1):53–61. doi:10.1016/j.apcata.2003.11.017.

34. van der Zande LM, de Graaf EA, Rothenberg G. Design and parallel synthesis of novel selective hydrogen oxidation catalysts and their application in alkane dehydrogenation. *Adv Synth Catal*. 2002; 344(8):884–889.
35. Rothenberg G, De Graaf EA, Bliek A. Solvent-free synthesis of rechargeable solid oxygen reservoirs for clean hydrogen oxidation. *Angew Chem Int Ed*. 2003;42(29):3366–3368. doi:10.1002/anie.200351545.
36. De Graaf EA, Andreini A, Hensen EJM, Bliek A. Selective hydrogen oxidation in a mixture with ethane/ethene using cerium zirconium oxide. *Appl Catal A Gen*. 2004;262(2):201–206. doi:10.1016/j.apcata.2003.11.027.
37. De Graaf EA, Zwanenburg G, Rothenberg G, Bliek A. Two-step catalytic oxidative dehydrogenation of propane: an alternative route to propene. *Org Process Res Dev*. 2005;9(4):397–403. doi:10.1021/op050020r.
38. Beckers J, Drost R, Van Zandvoort I, Collignon PF, Rothenberg G. Selective hydrogen oxidation in the presence of C3 hydrocarbons using perovskite oxygen reservoirs. *ChemPhysChem*. 2008;9(7): 1062–1068. doi:10.1002/cphc.200800039.
39. Blank JH, Beckers J, Collignon PF, Rothenberg G. Redox kinetics of ceria-based mixed oxides in selective hydrogen combustion. *ChemPhysChem*. 2007;8(17):2490–2497. doi:10.1002/cphc.200700431.
40. Blank JH, Beckers J, Collignon PF, Clerc F, Rothenberg G. A "green route" to propene through selective hydrogen oxidation. *Chem A Eur J*. 2007;13(18):5121–5128. doi:10.1002/chem.200601588.
41. Mattisson T, Jing D, Lyngfelt A, Rydén M. Experimental investigation of binary and ternary combined manganese oxides for chemical-looping with oxygen uncoupling (CLOU). *Fuel*. 2016;164:228–236. doi:10.1016/j.fuel.2015.09.053.
42. Sofranko JA, Leonard JJ, Jones CA, Gaffney AM, Withers HP. Catalytic oxidative coupling of methane over sodium-promoted Mn/SiO_2 and Mn/MgO. *Catal Today*. 1988;3(2–3):127–135. doi:10.1016/0920-5861(88)87003-2.
43. Shafiefarhood A, Galinsky N, Huang Y, Chen Y, Li F. Fe_2O_3@-$La_xSr_{1-x}FeO_3$ core-shell redox catalyst for methane partial oxidation. *ChemCatChem*. 2014;6(3):790–799. doi:10.1002/cctc.201301104.

Manuscript received Oct. 24, 2017, and revision received Mar. 7, 2018.